ON THE PERFORMANCE OF A WING HAVING TIP CLEARANCE

PART I. THE CASE IN WHICH THE TIP CLEARANCE IS CONTAINED WITHIN A NON-UNIFORM FLOW

SHINTARO OTSUKA and YOSHIYUKI SUGIYAMA

Department of Aeronautical Engineering

(Received June 5, 1969)

Abstract

The purpose of this investigation is to consider the effect due to the tip clearance, such as in turbomachine blades, on the aerodynamic characteristics of the blade. An experimental study was made on a stationary wing (whose plan form was rectangular: chord length $c=70$ mm, blade span $b/2=290\sim300$ mm) with the clearance formed between the side wall of a wind tunnel and a wing tip which was placed in the boundary layer developed on the side wall. The measurements were carried out in forty-two cases of seven clearances and six angles of incidence. The thickness of the side wall boundary layer was about 16 mm in the upstream of $1.5c$ apart from the leading edge of the wing. An aspect ratio (b/c) of the wing was about 8.43. Chordwise pressure distributions on the wing surface were measured at twenty spanwise positions. The measured pressures were integrated graphically to obtain the lift and drag at each spanwise position.

The results obtained were as follows. Increases in lift and drag in the region adjacent to the tip result from the predominant suction pressure due to the clearance flow, and are affected by the angle of incidence. Decreases in lift in spanwise positions, beyond about $0.1c$ from the tip, result from the suction pressure weakened near the leading edge due to the clearance flow and side wall boundary layer. By the side wall boundary layer, the lift and drag are diminished in the inside and in the neighborhood of the layer.

1. Introduction

When we design axial flow machines, we have only a small amount of information about the complicated field of flow passing through the machine. For example, we know little about energy losses in the flow with the interaction of the tip clearance flow and the secondary flow, those losses are essential in estimating the energy losses in the flow passing through the machine.

Let us take an isolated, stationary wing of an untwisted, rectangular form, whose tip is within a non-uniform flow (its example is the boundary-layer flow developed on the side wall facing the wing tip). Even in this simple case mentioned above the disturbances due to the effects of the clearance flow and the so-called secondary flow, make it difficult to predict the wing characteristics.

The theoretical results hitherto obtained for a wing with small tip clearance scarcely agree with experiments even in a uniform flow[3]. On the other hand, there are many experimental studies of an isolated wing with tip clearance or secondary flow. The wing characteristics, however, based on the pressure distribution on the wing surface, especially in the neighborhood of the tip, have not

been investigated in detail taking into account the many factors (*e.g.* the aspect ratio, the angle of incidence etc.) which have to be considered.

The present investigation was intended to clarify experimentally the problems mentioned in the above paragraph. The authors measured in detail the pressure distribution on an isolated, stationary wing of an untwisted, rectangular form, whose tip is within the boundary layer developed on a side wall (facing the tip) of a low speed wind tunnel. The effects of the side wall boundary layer and clearance flow on the wing characteristics were considered in relation to the tip clearance and the angle of incidence.

Symbols

c : chord length

c_D : $= d \Big/ \left(\frac{1}{2}\rho U_0^2 c\right)$, drag coefficient

c_L : $= l \Big/ \left(\frac{1}{2}\rho U_0^2 c\right)$, lift coefficient

c_p : $= (p - p_0) \Big/ \left(\frac{1}{2}\rho U_0^2\right)$

d : drag per unit span

l : lift per unit span

p : pressure on wing surface

p_0 : reference static pressure in working section

p_s : static pressure

P_T : total pressure

s : tip clearance

u : velocity in side wall boundary layer

U : free stream velocity

U_0 : $= \sqrt{2(P_T - p_0)/\rho}$

x, z: co-ordinates (see Fig. 4)

y_t : distance from wing tip

α : angle of incidence (angle between lower surface of wing and direction of uniform flow)

δ : thickness of side wall boundary layer

δ^* : displacement thickness of side wall boundary layer

ξ, η: co-ordinates, $\eta = y_t + s$, (see Fig. 2)

ρ : air density

First suffixes	Second suffixes
l: lower surface	a: rear part of maximum thickness of wing profile
u: upper surface	h: front part of maximum thickness of wing profile
max: maximum	l: local
i: induced	

2. Apparatus and Procedure

Fig. 1 shows the low speed wind tunnel used. This has the bleed-off (1•2) around a section of the tunnel duct which is placed in the downstream of the contraction section (1•3). The total pressure of the tunnel stream is measured

with a total pressure tube (1•4). Fig. 2 indicates the details of the working section used. The angle of incidence α is set up by a side plate (2•4) and the tip clearance s is set up by thickness gauges. The wing (2•3) can move along a guide (2•2). Two taps (2•6) are the measuring taps of reference static pres-

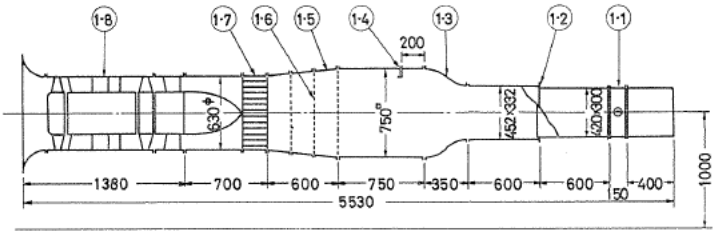

(1•1) Working section (1•3) Contraction section (1•5) Diffuser (1•7) Honeycomb
(1•2) Bleed-off (1•4) Total pressure tube (1•6) Gauze screens (1•8) Blower

FIG. 1. Wind tunnel used.

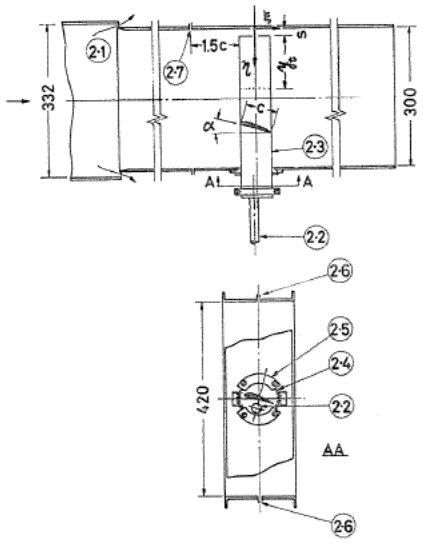

(2•1) Bleed-off
(2•2) Guide
(2•3) Wing for pressure measurement
(2•4) Side plate with angular scale
(2•5) Clamp
(2•6) Taps for measuring p_0
(2•7) Holes for boundary layer measurement

FIG. 2. Working section and nomenclature.

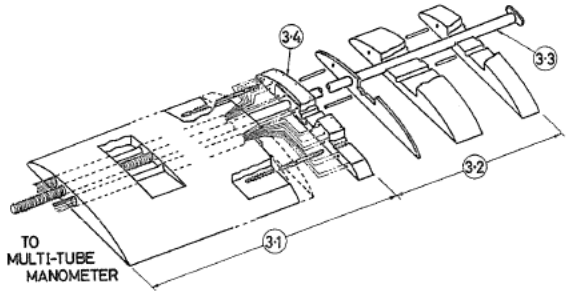

(3•1) Base wing (3•2) Wing segments (3•3) Shaft (3•4) Pressure holes

FIG. 3. Details of wing for pressure measurement.

sure (mentioned later). The velocity distribution over the tunnel section where the wing is to be mounted is almost uniform, except in the regions of the wall boundary layer.

Fig. 3 shows the details of the wing construction. This is an untwisted, rectangular wing and consists of a base wing (3·1) and additional wing segments (3·2). Their profiles are RAF 6 with a chord length of 70 mm. Their co-ordinates are given in Fig. 4, together with the co-ordinates of the pressure holes.

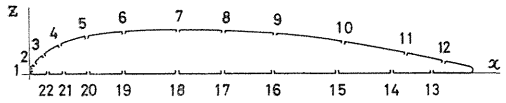

Co-ordinates of RAF 6 aerofoil

x%	0	2.5	5.0	10.0	20.0	30.0	40.0	50.0	60.0	70.0	80.0	90.0	100.0
z%	—	4.1	5.9	7.9	9.5	10.0	9.9	9.5	8.7	7.4	5.6	3.5	—

Leading-edge radius 0.7 R, Trailing-edge radius 0.54 R, Chord length $c=70$ mm.

Co-ordinates of pressure holes in the wing section

No.	1	2	3	4	5	6	7	8	9	10	11
x%	0.0	1.0	3.0	6.9	12.8	21.3	33.7	43.6	55.3	70.5	84.7
z%	0.9	2.9	4.7	6.8	8.6	9.6	10.0	9.7	9.0	7.2	4.6

12	13	14	15	16	17	18	19	20	21	22
93.2	90.6	81.6	69.2	54.9	43.7	33.4	21.2	13.1	7.6	4.2
2.7	0.0	0.0	0.0	0.0	0.0	0.0	0.0	0.0	0.0	0.0

FIG. 4. Wing section used and pressure holes.

The base wing can not be separated into wing segments. The base wing has twenty-two static pressure holes, 0.3 mm in diameter, at the distance of 1 mm from the tip. The wing segments and the major part of the base wing are made of brass, and the other part of the base wing shown by the dotted lines in Fig. 3 is made of epoxy resin. There are pressure tubes in the base wing. The pressure for the each hole is transmitted through the pressure tubes (0.7 mm in outer, and 0.5 mm in inner diameters) to a multi-tube manometer.

A series of wing segments is mounted on the tip of the base wing so that the distance between the pressure holes and the tip can be varied. The spanwise dimensions of the wing segments allow the pressure hole positions to be moved at 1 mm intervals within the span. A shaft (3·3) is used to fix the wing segments on the tip of the base wing.

The flow formed by the boundary layer developed on the side wall of the tunnel, was used as the "non-uniform flow".

The Reynolds number based on the wing chord was kept about 1.4×10^5 ($U_0\fallingdotseq$

30 m/s) at the working section throughout the experiments. The velocity distribution of the side wall boundary layer used is shown in Fig. 5. These data were obtained at the center of the side wall in the upstream of 1.5c from the leading edge of the wing. This is close to the 1/7th-power law, and varied scarcely in the range of α and s covered in the experiment.

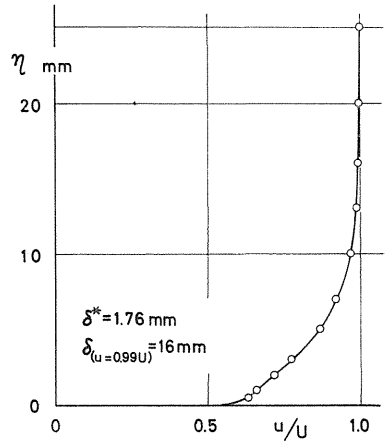

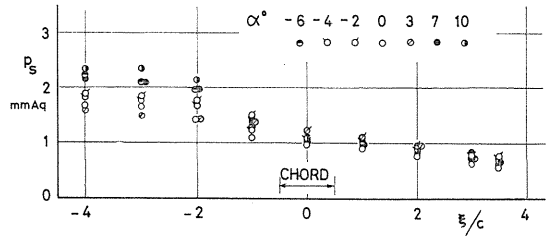

FIG. 6. Selection of reference pressure p_0.

← FIG. 5. Velocity distribution on side wall facing wing tip.

Fig. 6 shows the mean values of static pressures obtained along the center line of the upper and lower walls of the tunnel. It is evident from this figure that neglecting a deviation in pressure of about 0.2 mmAq from the mean value, the mean static pressures maintain approximately a steady value in the region $-(1/2) < (\xi/c) < (1/2)$ irrespective of the angle of incidence. Taking this into consideration, we selected the static pressure at the center of the working section ($\xi/c=0$ in Fig. 6) as the reference pressure p_0 and calculated the mean dynamic pressure at the working section as $\rho U_0^2/2 = P_T - p_0$. At an angle of incidence above about $\alpha=13°$, the results in Fig. 6 do not hold true.

The experiments were made over a range covering $\alpha=6$, 3, 0, -2, -4, $-6°$; $s=0$, 1, 2, 3, 5, 7, 10 mm, for a side wall boundary layer thickness of about 16 mm (illustrated in Fig. 5) and an aspect ratio (b/c) of about 8.43. The chordwise pressure distribution data were taken at twenty places along the span. Pressures were recorded by photographing the water columns of the multi-tube manometer. The pressure distributions were integrated by means of a planimeter to obtain $c_N = N \Big/ \left(\frac{1}{2}\rho U_0^2 c\right)$ and $c_C = C \Big/ \left(\frac{1}{2}\rho U_0^2 c\right)$, where $N = \int_0^c (p_u - p_l)dx$, $C = \int_0^{z_{max}} (p_{ua} - p_{uh})dz$. Thus we were able to get c_L and c_D as follows:

$$c_L = c_N \cos\alpha - c_C \sin\alpha, \quad c_D = c_N \sin\alpha + c_C \cos\alpha.$$

The values of c_L and c_D are directly proportional to local lift and drag, respectively. The local lift- and drag coefficients based on local dynamic pressure can be calculated by the expressions $c_{Ll} = c_L U_0^2/(U^2 \text{ or } u^2)$, and $c_{Dl} = c_D U_0^2/(U^2 \text{ or } u^2)$, respectively.

Fig. 7 shows the comparison between some wing characteristics obtained from our experiments and those of the two-dimensional aerofoil with the same profile as we used. According to Fig. 7, the above method of calculating the wing characteristics from the experimental results is justified. Although there is some small discrepancy between the experimental and two-dimensional values of c_D in Fig. 7, this can be explained as follows: α varies only in a small angle (w_s/U) with induced secondary velocity w_s due to the side wall boundary layer. This leads to a new value of lift $l'=l\cdot\cos(w_s/U)\fallingdotseq l$ and to the additional induced drag $d_i=l\cdot\sin(w_s/U)\fallingdotseq l\cdot(w_s/U)$. Therefore the new value of drag d' amounts to $d+d_i$.

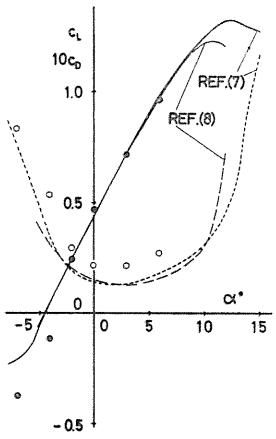

FIG. 7. Two-dimensional characteristics of RAF 6 aerofoil used ($R_e=1.8\sim3.3\times10^5$; ——— c_L, ····· c_D), and comparison between those and present experiments ($s=0$, $y_t=150$ mm, $R_e=1.4\times10^5$; ● c_L, ○ c_D).

Finally the authors make a remark that the aerodynamic effect of the upper and lower walls of the wind tunnel can be neglected in the type of tunnel used in our experiment because of ref. (9).

3. Results and Considerations

3.1. Chordwise pressure distributions

3.1.1. The positive angles of incidence

Fig. 8 (a) gives an example of the variation of chordwise pressure distributions against α and s at various spanwise positions. Since at $y_t=180$ mm, there is little influence due to the tip clearance and side wall boundary layers on the pressure distributions, the pressure distributions at $y_t=180$ mm serve as a standard in comparing with other distributions at any y_t.

(a) The upper surface of the wing

There are two peaks in the pressure distribution near the tip. One is near the leading edge and approaches to the leading edge as s decreases. The other is near the trailing edge and draws closer to the trailing edge as s increases. The causes of these phenomena are not the same. The former is due to such suction pressure as in the neighborhood of the leading edge for two-dimensional aerofoils, while the latter is due to the separation of the clearance flow at the sharp corner formed by the upper surface and the end plane of the wing. The peak suction pressure of the latter develops with increasing α and s. The generation of the suction pressure in the rear part of the wing profile leads to an increase in drag.

It is also seen that in $s=(3\sim5)$ mm, the suction pressure near the trailing edge and in the portion at $y_t<5$ mm increases suddenly. This phenomenon indicates that the clearance flow develops suddenly between $s=3$ mm and 5 mm. The magnitude of the suction peaks near the trailing edge and near the tip (about

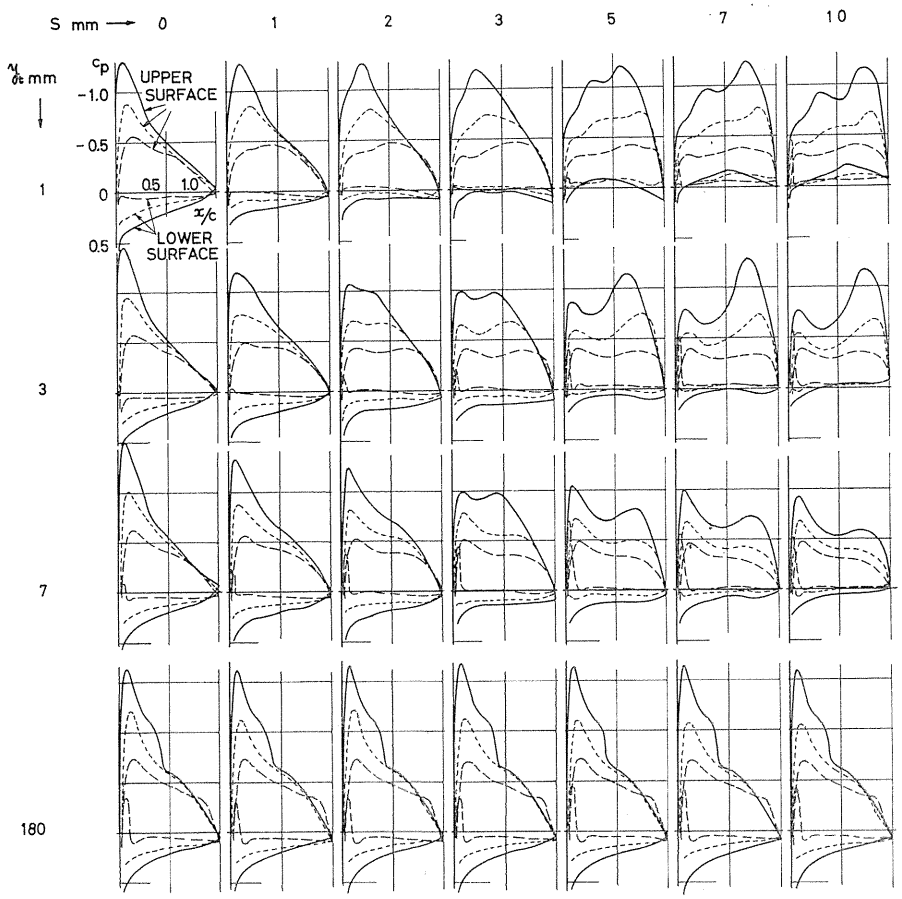

FIG. 8 (a) Chordwise pressure distributions at various spanwise positions (—— $\alpha=6°$, ---- $\alpha=3°$, - - - $\alpha=0°$).

$y_t<5$ mm) increases with an increase in α. But the peak of the negative pressure near the leading edge for $s=0$ is larger than the peak for $s\neq 0$ at any y_t.

Further, the peak near the trailing edge is always smaller than that near the leading edge, except in cases of about $y_t<5$ mm and $s>5$ mm. In cases of about $y_t<5$ mm and $s>5$ mm, the peak near the trailing edge seems to have a maximum value at a certain value of s, and is always larger than that near the leading edge. When y_t and s are increased, there is a marked effect of the clearance flow which appears first at about $y_t=3$ mm and $s=2$ mm.

Considering the pressure distribution around $y_t=(1\sim 2)$ mm, we find that an indent at about the mid-chord position has a tendency to move towards the trailing edge as s increases. The movement of the indent can be explained from the fact that the clearance flow drifts along with the main stream flowing in the clearance, and consequently the area of the suction pressure due to the clearance flow is also moved towards the trailing edge.

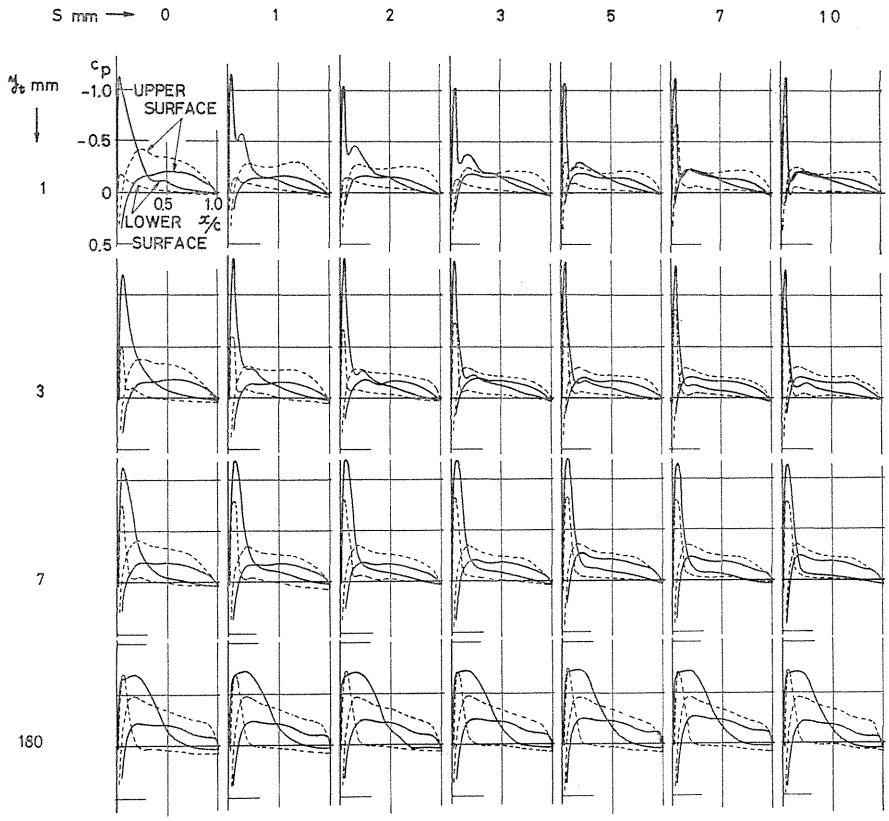

FIG. 8 (b). Chordwise pressure distributions at various spanwise positions (---- $\alpha=-2°$, —— $\alpha=-4°$).

(b) The lower surface of the wing

The pressure distributions on the lower surface change only mildly with s, α and y_t in comparison with those on the upper surface. As s increases, the (positive) pressure on the lower surface near the tip changes gradually into a weak suction pressure (see Fig. 8 (a), $y_t=1$ mm and $s=(3\sim10)$ mm), which disappears suddenly as y_t increases. The region in which the above mentioned reduction of the pressure exists (the region within $y_t=(1\sim3)$ mm), extends towards both the leading and trailing edge from the mid-chord position near the tip.

3.1.2. The negative angles of incidence (see Fig. 8 (b))

(a) The upper surface of the wing

The suction pressure on the upper surface is weakened with increases in s, and the suction pressure due to the clearance flow around the trailing edge is weakened with increases in $|\alpha|$.

(b) The lower surface of the wing

In the region of about $y_t=(1\sim10)$ mm, the pressure distribution has a main sharp suction peak which appears between about $(x/c)=0.04$ and 0.33 (the pressure hole No. 22 and No. 18, respectively), and especially at $\alpha=-4°$ ($-6°$), irregularity

is introduced by a second suction peak which appears on the slope of the rear side in the main sharp suction peak. The irregularity develops with increases in s and, at the same time, makes the main sharp suction peak grow sharper and sharper. It seems that the clearance flow which develops with increases in s and which passes through the clearance from the vicinity of the leading edge on the upper surface to the region between about $(x/c)=0.04$ and 0.33 (the pressure hole No. 22 and No. 18, respectively) on the lower surface, makes the above irregularity take place. The present data lead to the conclusion that there is a clearance flow even around the angle of the zero lift, provided that the pressure distribution has local unbalance between the upper and lower surfaces of the wing near the tip.

3.1.3. The effect of the side wall boundary layer

(a) The positive angles of incidence

With a positive angle of incidence the effects caused by the side wall boundary layer to the pressure distributions on the wing surface are as follows. Comparing the pressure distributions at $y_t=1$ mm with those at $y_t=180$ mm in the case of $s=0$ mm, we find that the effects from the side wall boundary layer are slight on the lower surface, but great over the upper surface, especially the suction pressure near the leading edge is weakened considerably. This results in the reduction of lifting force. It can be seen from $c_p\sim(z/c)$ curves in Fig. 9 that the side wall boundary layer reduces remarkably the (positive) pressure between about $(x/c)=0$ and 0.01, *i.e.* between No. 1 and No. 2 pressure holes. The above tendency accompanied by the $c_p\sim(z/c)$ curves is quite similar to the case of the negative angles of incidence (mentioned next paragraph). This results in a decrease in drag.

(b) The negative angles of incidence

With negative angles of incidence, the effects of the side wall boundary layer on the pressure distribution can be found from the distributions for $s=0$ in Fig. 8 (b) as follows.

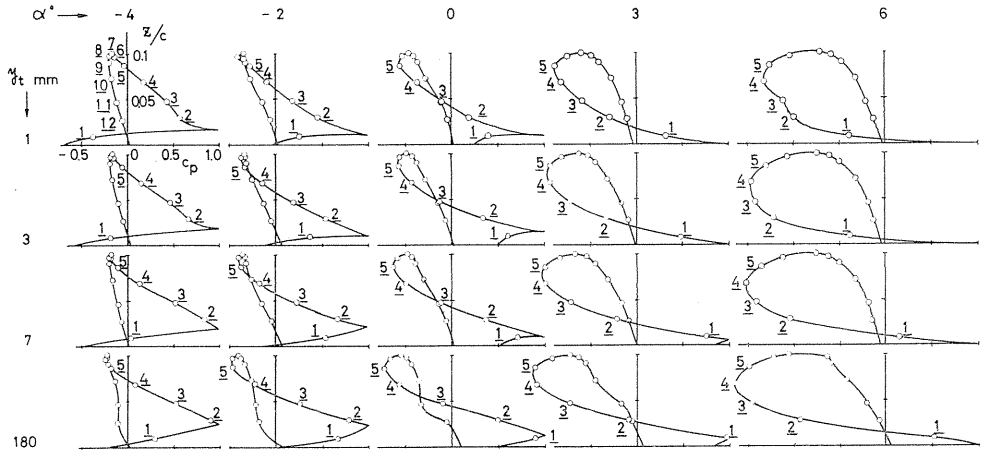

FIG. 9. Pressure distributions for $s=0$ on a plane perpendicular to the chord at various spanwise positions and angles of incidence. (Underlined figures show the number of pressure holes on the wing surface.)

On the upper surface the suction pressure in two regions (between about $(x/c)=0.07$ and 0.44 and between about $(x/c)=0.85$ and 0.93) is weakened at any α by the side wall boundary layer.

On the lower surface, when $|\alpha|$ is small ($\alpha \fallingdotseq -2°$), a sharp suction pressure between about $(x/c)=0.04$ and 0.21 develops with increase in y_t, while the other portion of the pressure distribution keeps its original form with slight pressure rises with increase in y_t. In the case of large $|\alpha|$ (that is, $\alpha=-4°$ (or $-6°$ which case is not shown in the figure)) a region with a very sharp suction pressure occurs between about $(x/c)=0.04$ and 0.33 in the side wall boundary layer. On the other hand, out of the side wall boundary layer (see the case of $y_t=180$ mm), the very sharp suction pressure mentioned above is weakened considerably in comparison with that in the side wall boundary layer. In addition to this phenomenon, the pressure on the front part of the lower surface (about $x/c<0.20$) except in the immediate neighborhood of the leading edge reduces considerably out of the side wall boundary layer.

Let us consider why the change of pressure distributions mentioned above occurs in the case of large $|\alpha|$. When $|\alpha|$ is large, the air flow along the wing surface turns abruptly from the upper surface to the lower surface around the leading edge. The effects due to the turning flow mentioned above are different between the inside of the side wall boundary layer and the outside of the layer.

Firstly, let us consider the turning flow in the side wall boundary layer. We can see from Fig. 8 (b) that the very sharp suction peak, which is followed by a steep adverse pressure gradient, occurs within a short distance from the stagnation point. Though the boundary layer around the very sharp suction peak mentioned above will be most likely a laminar one which separates easily from the wing surface under a positive pressure gradient, the disturbance due to the side wall (turbulent) boundary layer will force the wing-surface boundary layer to make a transition from laminar to turbulent state. This will suppress the laminar separation of the layer from the wing surface, and will keep the very sharp suction peak near the leading edge.

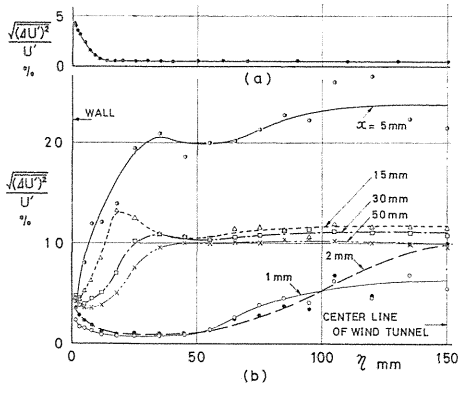

FIG. 10. Measurement of fluctuating turbulent component (a) at position of 1.5 c upstream of leading edge of wing ($\alpha=-4°$, $s=0$), (b) at various span- and chordwise positions of about 0.7 mm from lower surface of wing ($\alpha=-4°$, $s=0$). Root-mean-square of longitudinal fluctuation $\sqrt{(\Delta U')^2}$, local mean velocity U'.

Secondly, out of the side wall boundary layer, the factors to make a transition of the wing-surface boundary layer from laminar to turbulent state are not so predominant. This causes the laminar boundary layer on the wing surface to

separate from the surface, and so the height of the very sharp suction peak decreases. After the separation, turbulent mixing increases, and then the flow once more attaches itself to the wing surface. These processes in the flow along the wing will produce the pressure distribution mentioned above in the case of large $|\alpha|$. Fig. 10 (b) which shows the measurement of a fluctuating turbulent component at positions of about 0.7 mm from the lower surface of the wing, supports the above explanation of the effect from the side wall boundary layer.

3.2. Spanwise distributions of lift

Fig. 11 indicates the variations of c_L against η obtained by the integration of the pressure distributions.

3.2.1. The case of positive lift

There is an increase in lift in the region $y_t(=\eta-s)<(5\sim7)$ mm[2)4)]. This is due to the suction pressure caused by the clearance flow. Of course, it is near the trailing edge on the upper surface that the suction pressure mentioned above exists. This additional lift increases with increase in s and α. We do not know whether lift exists at the tip ($\eta=s$) or not. The phenomenon of the lift increasing in the immediate neighborhood of the tip, occurs also on a wing of finite length in free air[11)].

It seems that the reduction of lift at $y_t(=\eta-s)>(5\sim7)$ mm is caused by the facts that 1) the suction pressure due to the clearance flow is restricted within the immediate neighborhood of the tip; 2) the clearance flow forces the pressure to rise in the upper surface of the wing, except in the immediate neighborhood of the tip (see Fig. 13); and 3) the effect of the secondary flow due to the side wall boundary layer extends beyond the thickness of the side wall boundary layer.

At about $\alpha>(0\sim3°)$ and in the region of about $y_t(=\eta-s)<3$ mm, the lift coefficient c_L increases with increase in y_t within about $y_t<2$ mm and decreases with increase in y_t (for 2 mm$<y_t<$3 mm). It seems that this change of c_L comes from the decrease in pressure into suction pressure on the lower surface in the immediate neighborhood of the tip (Fig. 8 (a) and Fig. 13).

On the other hand, at $\alpha=-2°$ the change of c_L mentioned in the above paragraph probably does not exist (see Fig. 11). This seems to mean that the effect of the clearance flow near the tip differs from the cases of $\alpha>(0\sim3°)$.

3.2.2. The case of negative lift

Let us consider the reason why, at $\alpha=-4°$ (or $-6°$) and in a region of about $y_t<70$ mm, a maximum value of c_L exists (see Fig. 11). In the neighborhood of the tip, the suction pressure on the lower surface is weakened with increase in y_t except around the leading edge (Fig. 8 (b)). This leads to increase in lift and a maximum value of c_L is obtained. Further increases in y_t cause the suction pressure around the leading edge in the lower surface to weaken in some degree, but there is considerable drop in pressure on the other parts of the wing surface (Fig. 8 (b)). This leads to decrease in lift. These facts explain why c_L-curves at $\alpha=-4°$ (or $-6°$) have the maximum value near the tip. Of course, the phenomena mentioned above are due to the clearance flow and side wall boundary layer. The pressure distribution on the upper surface changes very little with increase in η or y_t and therefore contributes very little to c_L.

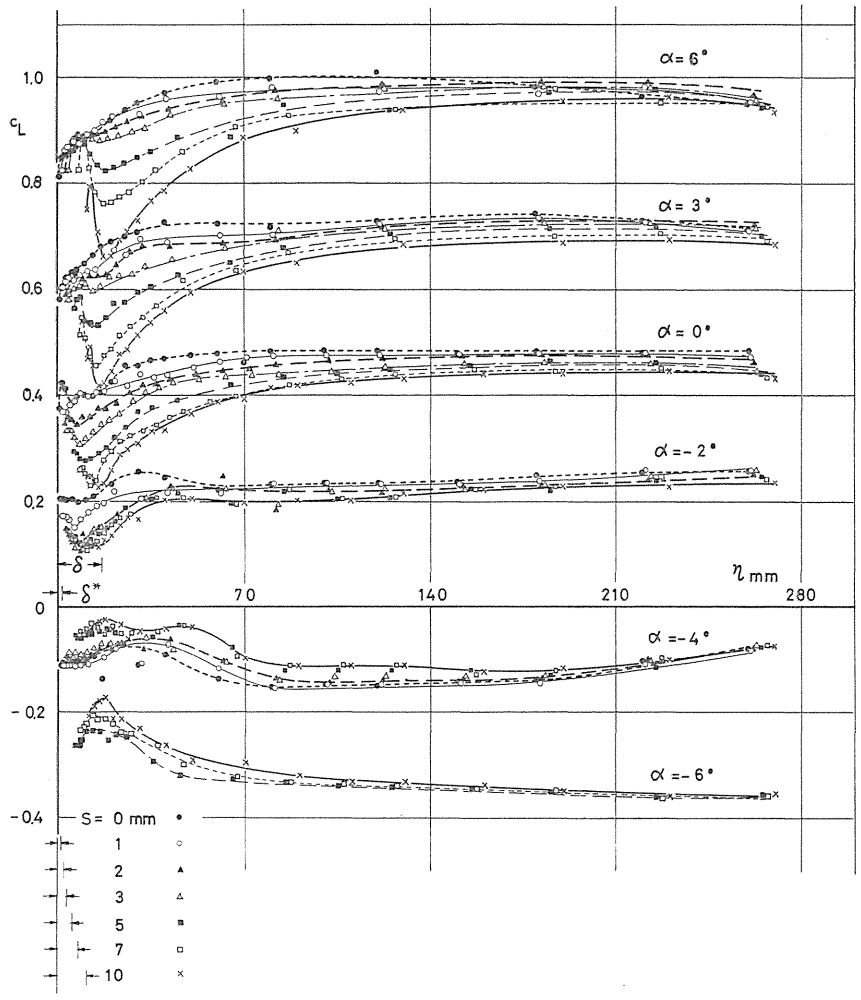

FIG. 11. Spanwise distributions of lift at various tip clearances and angles of incidence.

3.2.3. The effect of the side wall boundary layer

It is necessary to consider the effects of the side wall boundary layer on c_L. In this case we confine ourselves to the consideration of c_L-distribution for $s=0$. The decrease in c_L near the tip is due to the side wall boundary layer, whose influence on c_L has a tendency to increase as $|\alpha|$ increases. The region of decrease in c_L extends to the outside of the side wall boundary layer. This can be explained qualitatively from the fact that there is a reduction of lift resulting from downwash due to the secondary flow, which arises because of the side wall boundary layer.

3.3. Spanwise distributions of drag coefficient

The drag obtained by the integration of the pressure distribution is equal to

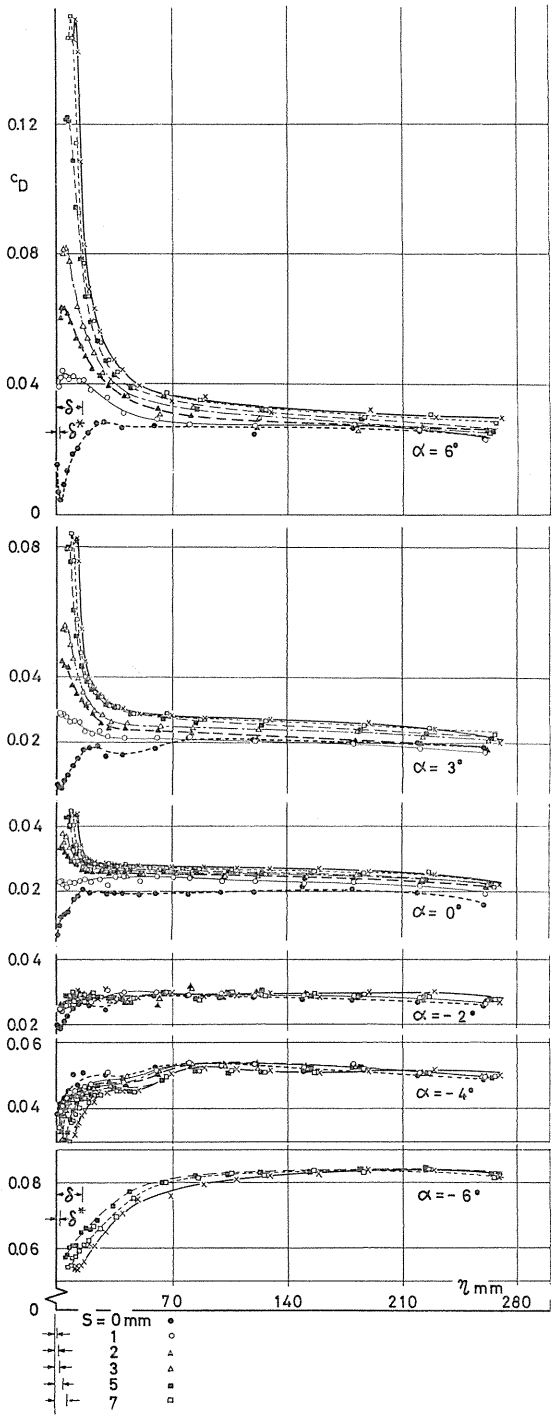

FIG. 12. Spanwise distributions of drag coefficient at various tip clearances and angles of incidence.

the sum of the induced drag and profile drag. Fig. 12 shows the variation of c_D against η.

3.3.1. The positive angles of incidence

Though c_D increases steeply with α and s in the region about $y_t(=\eta-s)<c/2$, the increase in c_D saturates at a certain value of s, and this s tends to increase as α increases. The variation in c_D against η in the region of $(\eta-s)>c/2$, is very mild and saturates also at a certain s. These seem to mean that the increase of the effect of the clearance flow with s ceases at a certain s. Of course, the rapid increase in c_D with decrease in η is attributed to the suction pressure which is due to the clearance flow on the upper surface in the neighborhood of the tip. The reason why the region of rapid increase in c_D with decrease in η is small, can be explained from the fact that the strong influence of the clearance flow is confined to a narrow area along the tip. At $\alpha=3°$ and $6°$, the drag coefficient c_D increases with increase in η within $(\eta-s)<2$ mm. The explanation for this is quite the same as in the case of c_L.

3.3.2. The negative angles of incidence

The decrease in c_D with decrease in η in the neighborhood of the tip is not so great as in the case of positive angles of incidence. In particular, c_D maintains almost the same value over the whole span at about $\alpha=-2°$ except when $s=0$.

3.3.3. The effect of the side wall boundary layer

Let us consider the effects of the side wall boundary layer in the case of $s=0$ (see Fig. 12). The decrease in c_D in the vicinity of the tip can be attributed mainly to the side wall boundary layer and this decrease tends to reach a minimum near the angle of zero lift (approximately $\alpha=-4.5°$ in RAF6 aerofoil). The range of decrease in c_D extends to the outside of the side wall boundary layer. This can be explained from the downwash due to the secondary flow caused by the side wall boundary layer.

3.4. Contours of pressure (isobar) (see Fig. 13)

3.4.1. The upper surface

The contours of pressure near the leading edge shrink remarkably towards the mid span of the wing because of the clearance flow, and the region with the predominant suction pressure due to the clearance flow drifts towards the trailing edge with an increase in s. Even in the case of $s=0$ the contours have lost their two-dimensional characteristic in the spanwise direction because of the effect of the side wall boundary layer. The contours around the tip in the case of $s=0$ are nearly equal to those in the case of $s=1$ mm, except some discrepancy in areas having the predominant suction pressure around the leading edge in the neighborhood of the tip. (The same tendency appears on the lower surface.) In other words, the clearance flow is predominant near the leading edge where great pressure difference exists between the upper and lower surface, while the effect of the clearance flow on other areas is small. It seems that this is due to the fact that the motive force generating the clearance flow is equal to the difference between the force due to the pressure difference $|p_u-p_l|$ near the tip and the re-

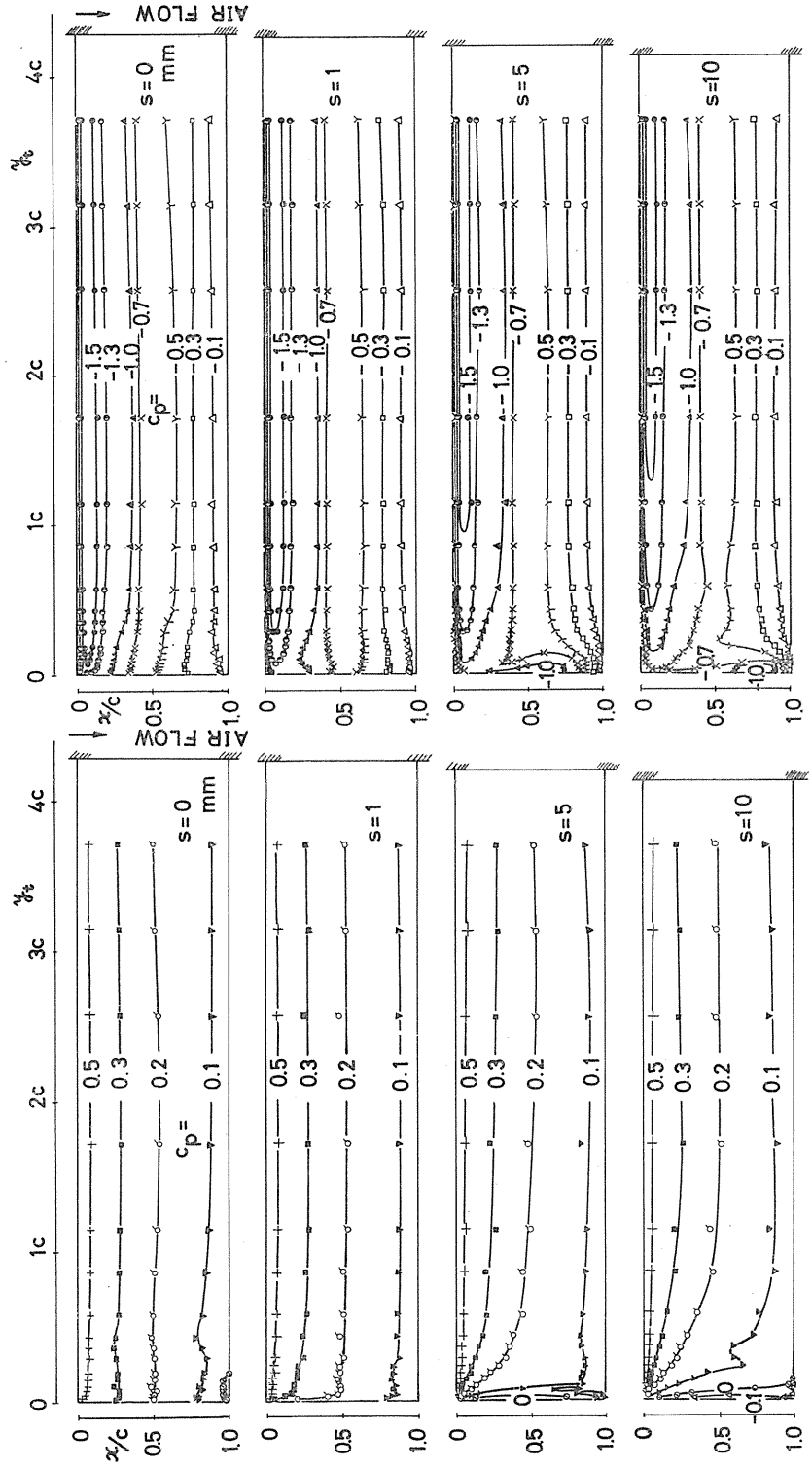

FIG. 13. Contours of pressure on wing surfaces at various tip clearances ($\alpha = 6°$).

sistance force due to the viscous effect of air in the clearance.

3.4.2. The lower surface

The region with the suction pressure in the immediate neighborhood of the tip spreads with an increase in s, and at the same time the suction pressure also develops. The contours at large s (about $s>3$ mm) diverge on the surface within $0<y_t<c$ from a corner formed by the leading edge and the tip-chord line, and have the form of parallel lines to the η-axis within $y_t>c$. The contours in the vicinity of the corner mentioned above are approximately independent of s except at small s (about $s<2$ mm). In the case of $s=0$, the contours tend to be distorted slightly on account of the side wall boundary layer within about $0<y_t<c$. In the case of $s=(1\sim2)$ mm the contours begin to curve towards the corner mentioned above in the vicinity of the tip, maintaining the tendency mentioned in the case of $s=0$ at the remainder part.

4. Conclusions

The pressure distributions on the wing surface near the tip depend upon the clearance flow and side wall boundary layer, to be more precise, we can say as follows:

(1) The predominant suction pressure due to the clearance flow occupies a narrow area near the tip section, and the region of the above suction pressure moves towards the trailing edge with increase in s. The suction pressure and its region depend upon α. Further, the predominant suction pressure causes an increase in lift on the wing surface within a short distance from the wing tip, and also an increase in drag on the wing surface within the region about $0<y_t<c/2$.

(2) In the case of positive lift, the reduction of lift with increase in s on the wing surface adjacent to the region with the additional lift mentioned in (1), is mainly due to the fact that the clearance flow greatly prevents a development of the suction pressure (corresponding to the suction pressure near the leading edge in a two-dimensional aerofoil) near the leading edge on the upper surface.

(3) In the case of $s=0$, the side wall boundary layer makes the lift and drag decrease on the wing surface not only in the inside but also in the outside of the layer.

(4) The clearance flow exists even around the angle of zero lift, because the pressure distribution around the tip has local unbalance between both surfaces of the wing.

Acknowledgments

The authors wish to acknowledge their indebtedness to Mr. F. Niwa and H. Muroi of the Department of Aeronautial Engineering, and Y. Hiramatsu of Toyohashi Technical High School, for their kind help in experiments.

References

1) W. R. Hawthorne: Rotational Flow through Cascades, Part I, The Components of Vorticity, Quart. J. Mech. appl. Math., 8-3 (1955-9), 266.

2) B. Lakshminarayana and J. H. Horlock: Tip-Clearance Flow and Losses for an Isolated Compressor Blade, ARC R & M, No. 3316 (1963).
3) B. Lakshminarayana: Effects of a Chordwise Gap in an Aerofoil of Finite Span in a Free Stream, J. roy. aeron. Soc., **68** (1964), 276.
4) R. Hürlimann: Untersuchungen über Strömungsvorgänge an Schaufelenden in der Nähe von Wänden, Diss. E. T. H. Zürich, (1963).
5) D. Mehmel: Die Spaltströmung an Geraden Schaufelgittern, Ing.-Arch., **31**-4 (1962), 294.
6) O. Flachsbart: Spaltverluste an Tragflügeln, Z. angew. Math. Mech., **11**-6 (1931), 411.
7) The Investigations on the Characteristics of the Aerofoils (I), Report of the Aeroplane Division, The Aeronautical Laboratory of the Japan Navy, (1938), (in Japanese).
8) The Investigations on the Characteristics of the Aerofoils for Propeller Use, Report of the Scientific Division, The Aeronautical Laboratory of the Japan Navy, (in Japanese).
9) L. Rosenhead: The Lift on a Flat Plate between Parallel Walls, Proc. roy. Soc. Lond., Ser. A, **132** (1931), 127.
10) D. Küchemann: The Effects of Viscosity on the Type of Flow on Swept Wings, Proceedings of a Symposium held at N. P. L., Her Majesty's Stationery Office, (1955).
11) L. Prandtl and O. G. Tietjens: Applied Hydro- & Aeromechanics, (1957), 158, Dover Pub., Inc., (New Dover edition).